Investigation of the efficiency of BiOI/BiOCl composite photocatalysts using UV, cool and warm white LED light sources - photon efficiency, toxicity, reusability, matrix effect, and energy consumption

Máté Náfrádi, Klara Hernadi, Zoltán Kónya, Tünde Alapi

PII: S0045-6535(21)01107-3

DOI: https://doi.org/10.1016/j.chemosphere.2021.130636

Reference: CHEM 130636

To appear in: *ECSN*

Received Date: 31 January 2021

Revised Date: 10 April 2021

Accepted Date: 19 April 2021

Please cite this article as: Náfrádi, M., Hernadi, K., Kónya, Z., Alapi, T., Investigation of the efficiency of BiOI/BiOCl composite photocatalysts using UV, cool and warm white LED light sources - photon efficiency, toxicity, reusability, matrix effect, and energy consumption, *Chemosphere*, https://doi.org/10.1016/j.chemosphere.2021.130636.

Author contributions:

Tünde Alapi: Conceptualization, Writing- Reviewing and Editing

Máté Náfrádi: Experimental work, Data evaluation, Writing

Klára Hernádi: Conceptualization

Zoltán Kónya: Providing XRD, DRS and XPS measurements

Investigation of the efficiency of BiOI/BiOCl composite photocatalysts using UV, cool and warm white LED light sources - photon efficiency, toxicity, reusability, matrix effect, and energy consumption

Máté Náfrádi[1], Klara Hernadi[2,3], Zoltán Kónya[2], Tünde Alapi[1]*

[1] Department of Inorganic and Analytical Chemistry, University of Szeged, H-6720 Szeged, Dóm tér 7. Hungary

[2] Department of Applied and Environmental Chemistry, University of Szeged, H-6720 Szeged, Rerrich Béla tér 1. Hungary

[3]Institute of Physical Metallurgy, Metal Forming and Nanotechnology, University of Miskolc, HU-3515 Miskolc-Egyetemváros, Hungary

**Email: alapi@chem.u-szeged.hu*

**Corresponding author*

ABSTRACT

BiOI, BiOCl, and their composites (BiOI:BiOCl) with molar ratios from 95:5 to 5:95 were synthesized and tested in the transformation of methyl orange (MO) and sulfamethoxypyridazine (SMP) antibiotic, using three various LED light sources: UV LEDs (398 nm), cool and warm white LEDs (400 - 700 nm). The 80:20 BiOI:BiOCl photocatalyst showed the best adsorption capacity for MO and enhanced activity compared to BiOI and BiOCl. The apparent quantum yield (Φ_{app}) of the MO and SMP transformation for cool and warm white light was slightly lower than for 398 nm UV radiation. The effect of methanol and 1,4-benzoquinone proved that the transformation is initiated mainly via direct charge transfer, resulting in the demethylation of MO and SO_2 extrusion from SMP. The change of photocatalytic efficiency was followed during three cycles. After the first one, the transformation rates decreased, but there was no significant difference between the second and third cycles. The decreased efficiency is most probably caused by the intermediates, whose continuous accumulation was observed during the cycles. Ecotoxicity measurements

confirmed that no toxic substances were leached from the catalyst, but the transformation of both MO and SMP results in toxic intermediates. Using 80:20 BiOI:BiOCl and LED light source, the energy requirement of the removal is about half of the value determined using TiO_2 and a mercury vapor lamp. The effect of some components of wastewater (Cl^-, HCO_3^- and humic acids), pH, and two matrices on the composite photocatalysts' efficiency and stability were also investigated.

KEYWORDS

BiOX, photocatalysis, visible light, quantum yield

HIGHLIGHTS

- BiOI:BiOCl composites were synthesized and tested for photocatalytic applications
- the efficiency of three different LED light sources was compared for excitation
- adsorption capacity and transformation efficiency for MO are highly correlated
- 400-700 nm and 398 nm light are similarly efficient for BiOI:BiOCl excitation
- wastewater matrices and their components affect the adsorption and efficiency

Graphical Abstract

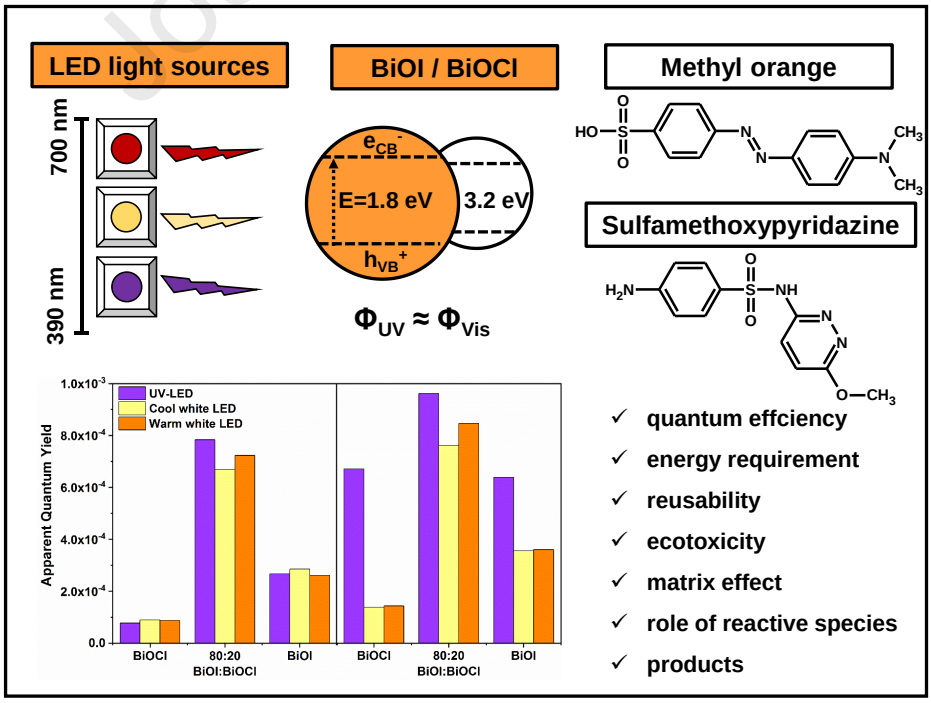

1. INTRODUCTION

One of the current water treatment challenges is developing cost-effective post-treatment methods to remove hazardous, non-biodegradable contaminants having biological activity. Advanced Oxidation Processes (AOPs), as additive water treatment methods, offer a solution to this problem (Khan et al., 2019; Stefan, 2017). One of the widely investigated processes is heterogeneous photocatalysis, which is based on semiconductors' application. The widely used photocatalysts, TiO_2 and ZnO having wide band gaps; therefore, they are mainly active in the UV region (Konstantinou and Albanis, 2003), and the transformation of the organic substances is generally initiated by hydroxyl radical. Due to the absorption of a photon having appropriate energy, an electron (e_{cb}^-) in the excited conduction band and a hole (h_{vb}^+) in the valence band form and initiates the transformation of organic substances (Qian et al., 2019). The transformation can take place via direct charge transfer (Ahmed and Haider, 2018), photosensitization (Akpan and Hameed, 2009), or reaction with reactive oxygen species (ROS) (Konstantinou and Albanis, 2003). Their relative contribution to the transformation of target pollutants depends on the photocatalyst's chemical and surface properties, the substrate's properties, and the reaction parameters.

One of the main goals from a material science perspective is the synthesis of catalysts, which efficiently work under visible light radiation, as sunlight is our cheapest and inexhaustible energy source. Bismuth oxyhalides (BiOX: X=F, Cl, Br, I), as photoactive materials, have received widespread attention during the last decade. BiOF and BiOCl are active in the UV range (band gap: 3.6 eV for BiOF and 3.2 eV for BiOCl), while BiOBr, and especially BiOI are active in the visible range (band gap: 2.6 eV for BiOBr and 1.8 eV for BiOI) (Singh et al., 2018; Bárdos et al., 2020). Their advantages include excellent adsorption capacity, they are easy to synthesize, but the fast recombination of photoinduced charges

decreases their efficiency (Cheng et al., 2014; Yao et al., 2020). Several attempts have been made to enhance the efficiency of BiOX photocatalysts, including the preparation of the composite catalysts. Composite materials, such as BiOCl/BiOBr (Jia et al., 2015; Zhang et al., 2020), BiOCl/BiOI, (Dong et al., 2012; Jiang et al., 2015; Shan et al., 2018; Siao et al., 2018; Wu et al., 2020; Xiao et al., 2012; Yang et al., 2016; Zhang et al., 2020; Zhong et al., 2018), SiO_2/BiOX (Shen et al., 2015) and TiO_2/BiOX (Dai et al., 2011; Liu et al., 2019), with improved stability and enhanced visible-light activity, were successfully synthesized. The activity improvement of the composite catalysts is explained by the synergetic effects of ion doping and heterostructure (Wang et al., 2020), the reduced recombination of electron-hole pairs (Shan et al., 2018), and highly enhanced adsorption capacity (Yang et al., 2016; Zhang et al., 2016, 2020). Methods such as the size-controlled synthesis of BiOX photocatalysts and the use of environmentally friendly, green synthesis methods were also investigated (Bárdos et al., 2019; Garg et al., 2018a, 2018b). Several studies are available about the structure, properties, and activity of BiOX photocatalysts. However, the effects of various reaction parameters that determine practical applicability, such as inorganic and organic wastewater components, and pH, have been rarely studied.

Due to the intensive development of optoelectronics in recent years, the use of light-emitting diodes (LEDs) radiating in the UV and visible light range has become increasingly popular. It makes possible improved efficiency of additive water treatment methods based on photochemical processes (Chen et al., 2017; Sergejevs et al., 2017). Compared to the conventional UV and visible light sources, LEDs have higher electric efficiency, lower price, better mechanical tolerance, and longer lifetimes; therefore, they are a promising option for application in water treatment processes, which requires either visible or UV radiation (Jo and Tayade, 2014).

The present study aims to prepare composites BiOCl/BiOI photocatalyst with different molar ratios, to determine their absorption properties and photocatalytic activity, and to compare the apparent quantum yields using different LED light sources (398 nm UV, cool and warm white light). For evaluation of the photocatalytic performance of the pure BiOI, BiOCl, and the composites, the methyl orange (MO) dye and sulfamethoxypyridazine (SMP) antibiotic degradation was chosen. Toxicity measurements have also been performed to investigate the potential risk of using these photocatalysts. Also, studies of the effects of Cl^-, HCO_3^-, humic acid, pH and two matrices (river water and biologically treated domestic wastewater) provide information on the practical applicability of the best composite photocatalyst.

2. MATERIALS AND ANALYTICAL METHODS

2.1. Materials

For the synthesis of photocatalysts, bismuth nitrate pentahydrate ($Bi(NO_3)_3 \times 5\ H_2O$, Alfa Aesar, 98%), potassium iodide and chloride (KI and KCl, Molar Chemicals, 99.7%), ethylene glycol (Sigma-Aldrich, 99.95%) and ethanol (VWR, 96%) were used without further purification. When the effect of additives was studied, NaCl (VWR, 99%), sodium-humate (Sigma Aldrich, tech. grade), methanol (VWR, 99.9 %), and 1,4-benzoquinone (Acros Organics, 99%) were used. The pH of the solutions was adjusted with H_2SO_4 (Fluka, 49-51%) or NaOH (VWR, 98%) and measured with InoLab p730 pH meter. Methyl orange (MO) from VWR, (99%), sulfamethoxypyridazine (SMP) from Sigma Aldrich (99%) were purchased. NaF was from Alfa Aesar (99%). O_2 or N_2 gas (Messer Hungarogáz, 99.5% and 99.995%) was used to keep constant dissolved O_2 concentration. For the actinometric measurements $Fe_2(SO4)_3$ (VWR, 98%), potassium oxalate (Reanal, 98%), ammonium-reineckate (Sigma

Aldrich, 93%), 1,10-phenanthroline (Sigma Aldrich, 99%), KOH (Fluka, 98%) and KSCN (VWR, 98%) was used.

Table S1 shows the date of matrices: river water (from Tisza, Szeged, Hungary) and the biologically treated domestic wastewater (from the water treatment plant, Szeged).

2.2 Preparation of BiOI/BiOCl composite catalysts

The BiOI and BiOCl photocatalysts were prepared as described in the literature (Bárdos et al., 2019). $Bi(NO_3)_3 \times 5\ H_2O$, KCl, and KI were used for preparation via a solvothermal method. The $Bi(NO_3)_3 \times 5\ H_2O$ and KCl, or KI was dissolved in 50 cm^3 ethylene glycol with continuous stirring and heating (up to 45 °C). The suspension was heat-treated for 3 hours at 120 °C in a PTFE-coated steel autoclave. The solid material was washed with distilled water and ethanol, then vacuum-filtered with a 0.1 μm pore size filter (Durapore®, hydrophilic PVDF) and dried for 24 hours at 40 °C. The composite catalysts were prepared with the same method, with the addition of KCl and KI at the appropriate molar ratios. The molar ratios have been calculated to result in composites with 5.0 to 95.0 n/n% BiOI content. The color of the prepared materials changed from white to red, with increasing BiOI content (Fig. 2/a).

2.3 Photocatalytic test reactions

In each case, 100 cm^3 suspension was irradiated in a cylindrical glass reactor (inner diameter: 45 mm). For determination of the amount of adsorbed MO and SMP, the suspensions were stirred in the dark for 30 min before photocatalytic tests. The experiments were started by turning on the light source. O_2 or N_2 gas was continuously bubbled through the suspension to keep constants the dissolved O_2 concentration.

Fig. S2 shows the emission spectra of the LED light sources. Three different LED light sources were used; commercial 'UV' (LEDmaster, $\lambda_{emission}$= 398±10 nm, 288 lumens, 4.6 W),

145 'cool white' (LEDmaster, $\lambda_{emission}$=400-650 nm, 390 lumens, 4.6 W), and 'warm white'
146 (LEDmaster, $\lambda_{emission}$=400-700 nm, 600 lumens, 4.6 W). 1.0 m of LED tape (60 LED/meter)
147 was fixed on the inside of the aluminum, double-walled reactor having 66 mm inner diameter.
148 The reactors were equipped with a water cooling system to ensure the LEDs' constant light
149 output. The electrical power required to operate the LEDs was the same (4.6 W) in all cases;
150 thus, the efficiency of the photocatalysts was determined at the same electrical energy input.

151 A widely used and commercially available photocatalyst, TiO_2 Aeroxide P25® (Acros
152 Organics, 35-65 m^2 g^{-1} specific surface area) was used as a reference measurement. The
153 irradiation of TiO_2 was performed using a fluorescent mercury vapor lamp (Lighttech;
154 GCL303T5/UVA; 307 mm × 20.5 mm; 15 W) emitting in the 300-400 nm range (λ_{max} = 365
155 nm). The suspension was irradiated in a 500 cm^3 cylindrical glass reactor.

156

157 *2.4 Analytical methods*

158 The emission spectra of the LED light sources (Fig. S2) were recorded using a two-
159 channel fiber-optic CCD spectrometer (AvaSpec-FT2048) in the 180-880 nm wavelength
160 range. The photon flux of the light sources was determined using two chemical actinometry
161 methods: Reinecke's salt (Wegner and Adamson, 1966) and the widely applied ferrioxalate
162 (Hatchard and Parker, 1956) actinometry. Reinecke's salt actinometry can be involved mainly
163 in the range of visible light; the quantum yield of the photolysis of Reinecke's salt changes
164 from 0.311 to 0.270 in the 400 - 600 nm region (Kuhn et al., 2004). The 0.01 M solutions of
165 potassium-reineckate were prepared (Cornet et al., 1997). The photon flux was calculated
166 from the formation rate of SCN^- determined via spectrophotometry with excess $Fe(NO_3)_3$. The
167 molar absorption coefficient of FeSCN (3188 mol^{-1} dm^3 cm^{-1}) was determined from the slope
168 of its calibration curve.

The ferrioxalate actinometry can be used in the UV and near-UV region (254 - 500 nm). This method is based on the photoreduction of $K_3Fe(C_2O_4)_3$, and the quantification of the Fe^{2+} ions is performed by complexation with 1,10-phenanthroline. Within the range of 365 – 514 nm, the quantum yield of the Fe^{2+} formation changes from 1.2 to 0.93 (Kuhn et al., 2004).

The photocatalysts adsorb well the MO dye. NaF solution (0.5 cm^3, 0.5 M) was added to the samples (1.0 cm^3) for effective desorption of MO and its intermediates. After adding the NaF solution, the sample was kept for 10 minutes in the dark and finally centrifuged (Dragonlab, 15000 RPM), and filtered with syringe filters (0.22 µm, FilterBiO, PVDF-L). The recovery was checked with 2.0×10^{-4} M concentration of MO in 0.50 g dm^{-3} BiOCl and BiOI containing suspensions and was found to be 98(±1) % in both cases.

For spectrophotometric measurements, an Agilent 8453 UV-Vis spectrophotometer was used. The molar absorbance of MO (at 464 nm) and SMP (at 261 nm) is 25905 and 18990 mol^{-1} dm^3 cm^{-1}, respectively. KI solution was used to determine the concentration of dissolved I^-. The absorbance was measured at 226 nm, the molar absorbance of I^- at this wavelength was 13080 mol^{-1} dm^3 cm^{-1}.

HPLC measurements were performed with an Agilent 1100 HPLC equipped with a diode array UV detector (DAD) to separate the intermediates and determine MO and SMP concentration in the treated suspension. For MO containing samples, the stationary phase was a Kinetex 2.6u XB-C18 100A (Phenomenex) reverse phase column, while the mobile phase consisted of 40 v/v% acetonitrile (VWR, UPLC-grade) and 60 v/v% formic acid solution (0.1%). For SMP containing samples the same stationary phase was used, the mobile phase consisted of 12.5 v/v% acetonitrile and 87.5 v/v% formic acid. The flow rate of eluent was 0.70 ml min^{-1}, and the temperature was 25 °C. The products were determined via mass spectrometry (Agilent LC/MSD/VL with ESI source). Measurement was performed in

positive mode (3500 V capillary voltage, 75 V fragmentor voltage), the scan range was 100-500 AMU.

Ecotoxicity test (LCK480, Hach-Lange) based on the bioluminescence measurements of *Vibrio fischeri* bacteria were used to determine the acute ecotoxicity of the samples. The inhibition of bioluminescence was measured using a Lumistox 300 (Hach Lange) luminometer after 30 min. incubation time. For elimination of the formed H_2O_2, the catalase enzyme (2000-5000 unit mg^{-1}, Sigma Aldrich) was added to the samples in 2.0 mg dm^{-3} concentration.

The synthesized catalysts were characterized using powder X-ray diffractometry (XRD) (Rigaku Miniflex II, Cu Kα radiation source, 5.0-90.0 2Theta° range, with 4.0 2Theta° min^{-1} resolution). The specific surface area was determined via N_2 adsorption/desorption isotherms using a Quantachrome NOVA 2200 analyser. The pore size distribution was calculated by the BJH method. Diffuse reflectance spectroscopy (DRS) was performed using an Ocean Optics DH-2000 light source and Ocean Optics USB4000 detector. The band gap energy values were evaluated by the Kubelka-Munk approach and the Tauc plot (Tauc, 1968) and reinforced by the first derivative approach method (Flak et al., 2013). X-ray photoelectron spectroscopy (Kratos XSAM-800 apparatus, non-monochromatic Mg Kα X-ray source) was adopted to investigate the surface elemental composition.

3. RESULTS AND DISCUSSION

3.1 Characterization of the photocatalysts

The XRD patterns of the synthesized pure BiOX (X = Cl, I) and their composites were compared (Fig. 1). The diffraction peaks can be indexed to the tetragonal BiOI and BiOCl phase (Bárdos et al., 2019). In the case of 50:50 molar ratios, peaks of both components could be detected. The BiOI/BiOCl composites containing 20:80 and 80:20 BiOCl:BiOI molar

ratios exhibit the characteristic peaks of pure BiOI or BiOCl (the main component). Comparing the profiles of BiOI with BiOI:BiOCl composite having 80:20 molar ratio, it can be seen that the diffraction peaks slightly shift to the higher angles, corresponding to a smaller spacing distance between the different planes. The same phenomenon is less pronounced for BiOI:BiOCl composite having a 20:80 molar ratio. Moreover, the diffraction peaks of composite are broader than the corresponding peaks of pure BiOX, indicating the smaller crystallite sizes during heterogeneous growth (Ahern et al., 2015).

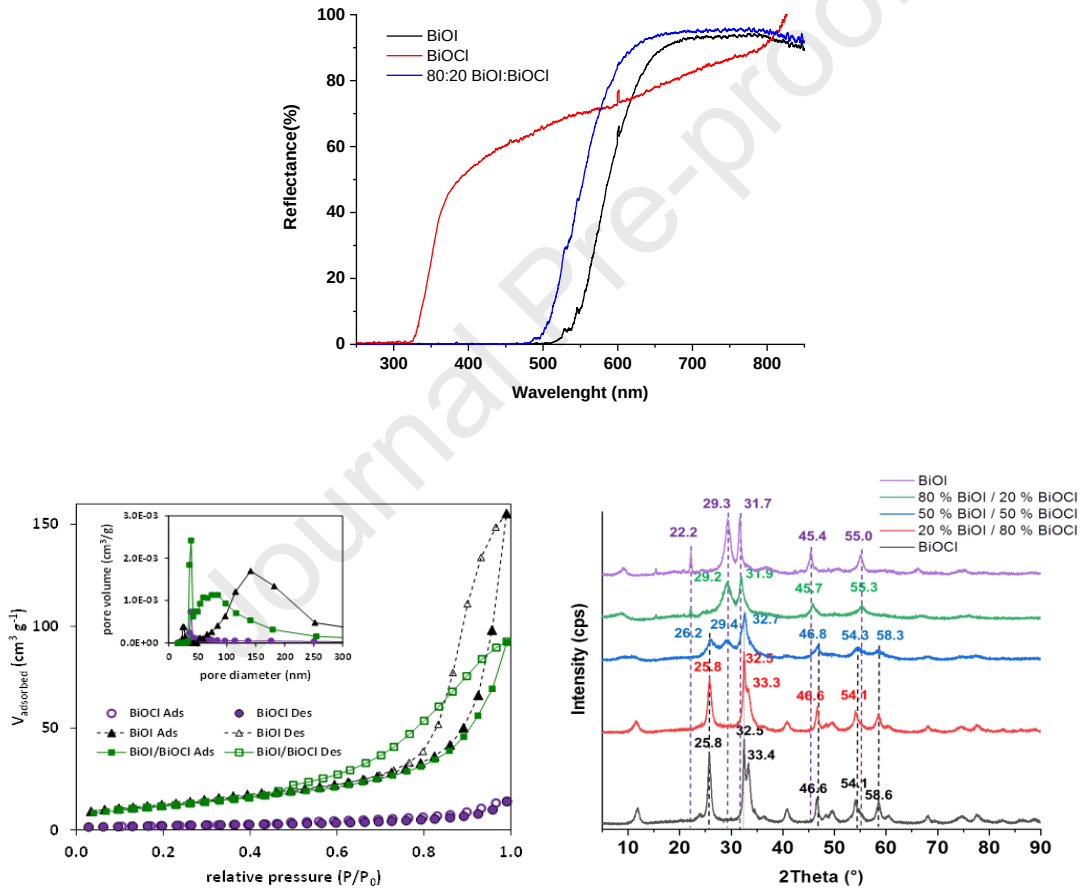

Fig. 1 UV-Vis DRS spectra, N_2 adsorption and desorption isotherms and the corresponding pore-size distribution (inset) and XRD patterns of BiOCl, BiOI, and their composites

Specific surface are of the photocatalysts, total pore volume and average pore diameter are presented in Table. 1. The hysteresis loop of the isotherm in the range of 0.6–1.0 P/P_0, (Fig. 1) suggests the formation of capillary condensation related to pores between closely-

packed particles. The surface area of BiOI is much larger than the surface area of BiOCl and is similar to that of a composite catalyst with 80% BiOI content (Table 1.).

Table 1 The specific surface areas, pore structures, band gap values and surface atomic composition of the photocatalysts

		BiOI	BiOCl	80:20 BiOI/BIOCl
Surface Area ($m^2 g^{-1}$)		45.7	7.4	43.1
Pore Volume ($cm^3 g^{-1}$)		0.15	0.015	0.10
Average Pore Size (nm)		141	38	39
Band gap (eV)		2.20	3.41	2.41
Surface atomic composition (%)	**O 1s**	31.1	15.1	25.7
	Bi 4f	20.4	20.6	22.7
	I 3d	13.8	-	12.6
	Cl 2p	-	21.3	2.6

To analyze the surface chemical composition X-ray photoelectron spectroscopy (XPS) were conducted. The overall surface chemical compositions including atomic concentrations of the major elements are listed in Table 1. The atomic ratio of I:Cl on the surface of the composite catalyst is 9.7:2; higher than 8:2, which was applied for the catalyst preparation, and indicates a high concentration of I^- on the surface. For BiOCl, the relative low atomic content of O 1s is due to the lack of surface hydroxyl group (Fig S1) (Di et al., 2016; Hao et al., 2017; Liu and Wang, 2016).

Fig 1 display the UV-Vis diffuse reflectance spectra of the BiOI, BiOCl and the 80:20 BiOI:BiOCl composite having best photocatalytic performance. While considering the optical properties of the investigated semiconductors the band gap energy for BiOCl was 3.41 eV, which is near to that reported in the literature (Ganose et al., 2016). Also, an interesting spectral feature was observed for this sample; its light absorption extends in the visible region. Although, this is unusual, it is not surprising as it can be related to the UV light induced formation of oxygen vacancies. This can be the reason of that, under UV radiation (even at

398 nm), the white color of BiOCl changes to gray, and then, after switching off the light, it returns to white in air. In the case of BiOI 2.20 eV was the band gap value, which is slightly different from what expected (~2.00 eV,(Ganose et al., 2016)). This means that Bi_5O_7I could be present in the sample, a material which is often a co-product of BiOI synthesis (Liu and Wang, 2016). For 80:20 BiOI/BiOCl composite, 2.41 eV, 0.2 eV higher band gap value was determined than that of BiOI sample, which points out the influence of BiOCl.

3.2 Characterization of the light sources

The light source usually determines the efficiency of each photochemical method. The emission spectra of the LED light sources are presented in Fig S2. The UV LED's photon flux emitting at 398±10 nm light was determined and compared by Reinecke'salt actinometry and ferrioxalate actinometry. Both methods can be applied for the determination of the photon flux of this light source. The values determined by Reinecke'salt actinometry was $5.81(\pm0.03)\times10^{-6}$ mol_{photon} s^{-1}, and a slightly lower value, $(5.12\pm0.02)\times10^{-6}$ mol_{photon} s^{-1} was obtained by ferrioxalate actinometry (Hatchard and Parker, 1956).

The photon flux was $3.47(\pm0.25)\times10^{-6}$ mol_{photon} s^{-1} for cool white LEDs, and $3.25(\pm0.25)\times10^{-6}$ mol_{photon} s^{-1} for the warm white LEDs. Both values were obtained by Reinecke's salt actinometry and were about 40 % of the UV LED's photon flux. Ferrioxalate actinometry provided much lower values since this method is suitable for determining the photon flux with a wavelength of shorter than 500 nm. In this way, the photon flux for cool white LEDs was $9.35(\pm0.65)\times10^{-7}$ mol_{photon} s^{-1}, about 20 % of the UV-LED's photon flux. This value was slightly lower ($7.76(\pm0.73)\times10^{-7}$ mol_{photon} s^{-1}) for the warm white LEDs. For calculation of the apparent quantum yield of the transformation, the photon flux determined by Reinecke'salt actinometry was applied.

3.3 Adsorption properties

Adsorption generally plays a crucial role in heterogeneous photocatalysis, especially in the conversion of dyes. The relative adsorbed amount of MO (2.0×10^{-4} M) in a suspension containing 0.5 g dm^{-3} catalyst was 29 % and 11 % for BiOI and BiOCl, respectively. This can be partly explained by the difference between the specific surface area (Table 1) and surface charge of BiOI and BiOCl. BiOI has a positive (Yusoff et al., 2019), while BiOCl particles possess negative surface charges over a wide pH range (Xiao et al., 2016; Zhao et al., 2018). MO is an azo dye with a pKa value of 3.46. The pH of the suspensions was 6.5, the MO was in deprotonated form having a negative charge. Due to the electrostatic interaction, adsorption of MO is most probably preferred on the surface of the BiOI. In the cases of the composite catalysts, the amount of adsorbed MO increased with increasing the BiOI content, up to 80:20 molar ratio, when 35.6(±2.5) % was adsorbed, and slightly decreased with the further increase of the BiOI content (Fig. 2/a). Adsorption of SMP was not measurable for either BiOI or BiOCl.

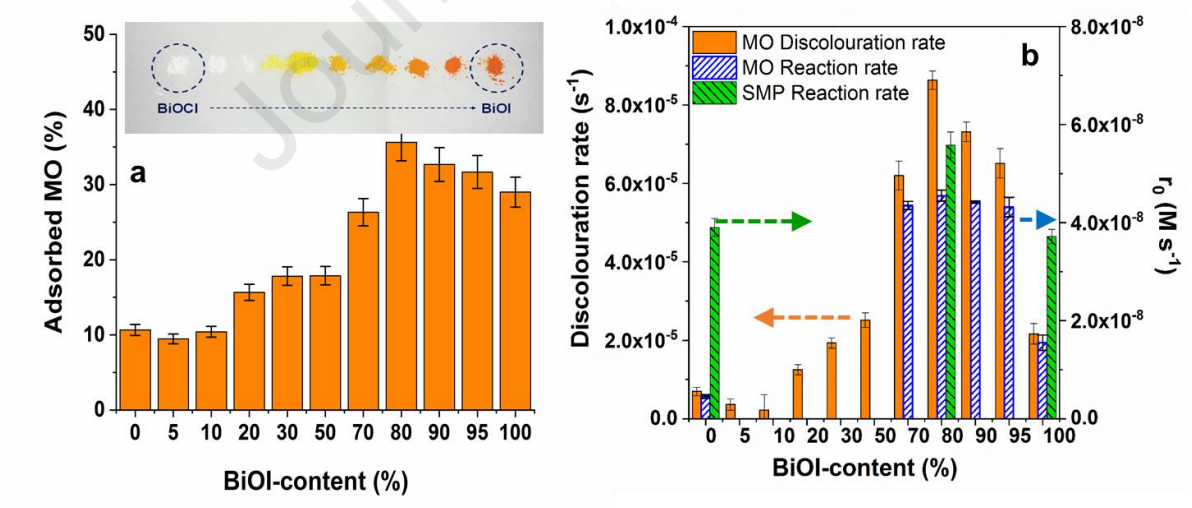

Fig. 2 The relative adsorbed amount of MO (2.0×10^{-4} M; 0.5 g dm^{-3} photocatalyst) (a), the rate of discoloration (based on the absorbance determined at 464 nm), and the initial reaction rate (r_0) of MO and SMP determined by HPLC-DAD (b) using photocatalysts having various BiOI content

3.4 The photocatalytic test reactions using UV LEDs

The relative contribution of the direct UV photolysis (398 nm irradiation) to the transformation of MO and SMP was negligible. The effect of suspension concentration on the transformation rate was investigated using 80:20 BiOI:BiOCl composite photocatalyst. Within the range of 0.5 - 1.5 g dm^{-3}, amount of adsorbed MO and its transformation rate increased linearly (Fig. S3). Similar trend was observed for SMP. In further experiments, 0.5 g dm^{-3} photocatalyst load was used to ensure adequate depth of light penetration into the suspension.

The interaction between the MO and the catalyst's surface requires the differentiation between the adsorbed and transformed amount of dye. Before determining MO concentration of the treated solution, NaF was added to the sample for desorption. In this way, the total amount of non-transformed MO can be measured. The initial transformation rate determined without NaF addition (2.40×10^{-8} M s^{-1}) is only 41 % of the value determined after the addition of NaF (4.10×10^{-7} M s^{-1}) to the samples (Fig. S4). Above ~40% conversion, there is no significant effect of NaF addition, which can be explained by the competitive adsorption between MO and its products. The transformation is likely to result in products that successfully compete with MO for adsorption sites. The pH of the suspension does not change significantly (from 6.5 to 6.2) during the transformation.

For MO, significantly increased activity was determined for the composite catalysts having more than 50% BiOCl content. The discoloration rate reached the maximum value in the range of 70-95% BiOCl content (Fig. 2b). Adsorption capacity and transformation efficiency are correlated (Fig. 2).

In the spectrophotometric measurements, the characteristic change of the shape of the MO spectrum and the shift of its maximum to the lower wavelengths indicates the formation of products having significant absorption around 400-450 nm (Fig. S6). Therefore, the HPLC-

DAD method was used to determine the initial transformation rate of MO for the most promising composite catalysts (70, 80, 90, and 95% BiOI content), the pure BiOI, and BiOCl (Fig 2b). For SMP, the HPLC-DAD method was used to determine the concentration in each case because of the formation of aromatic intermediates. The initial transformation rate of MO correlated with the discoloration rate: it was about three times higher for composite catalysts than for BiOI.

The photocatalytic activity of pure BiOCl, BiOI, and the 80:20 BiOI:BiOCl composite catalysts having the best adsorption properties were tested and compared using the UV LEDs (398 nm) light source. The initial transformation rate of MO was significantly higher for BiOI with a larger surface area and smaller bandgap value than for BiOCl. (Table 1). Surprisingly, the non-adsorbed SMP transformation takes place with similar rate in the case of both pristine photocatalysts. For BiOI, the transformation rate was doubled, while for BiOCl, a five time higher transformation rate was determined for SMP than for MO. The reason can be the UV light induced formation of oxygen vacancies in BiOCl and consequently extending the excitability to larger (above 363 nm) wavelength ranges. The composite catalyst showed increased activity to transform both components compared to the pure BiOI and BiOCl.

3.5 Comparison of the efficiency using UV, cool, and warm white LEDs

The activity of the catalysts were determined under visible light radiation, using cool white and warm white light and compared to the activity determined under 398 nm UV irradiation (Fig. 3). For both organic substances, the transformation rate was significantly higher using 398 nm irradiation than visible light, similarly, the product formation was markedly faster (Fig S5). Both BiOI and the composite catalyst proved better activity than BiOCl under visible light irradiation. There was no difference between the initial transformation rates determined in the case of cool white and warm white light. The excellent

behaviour of the composite was also manifested under excitation with visible light. Opposite to the BiOI:BiOCl composite catalyst, an induction period can be observed (up to 30 min.) when pure BiOI was used for MO degradation. During this period the transformation rate increased with the increased average energy of the photons (UV < Cool white < Warm white) (Fig S5).

Since there is a significant difference between the photon flux of each light source and the energy of the emitted photons, it is worth comparing the efficiency based on the apparent quantum yields (Φ_{app} = number of photons reached the treated suspension/number of molecule transformed) of the transformation. The photon flux of visible light LEDs ($3.47(\pm0.25)\times10^{-6}$ mol_{photon} s^{-1} for the cool and $3.25(\pm0.25)\times10^{-6}$ mol_{photon} s^{-1} for the warm white LEDs) is about 40% of the photon flux of UV LEDs ($5.81(\pm0.03)\times10^{-6}$ mol_{photon} s^{-1}). Also, photons' average energy is lower, as these LEDs emit light primarily in the 400-700 nm range. The flux of photons with a wavelength shorter than 500 nm for cool ($9.35(\pm0.65)\times10^{-7}$ mol_{photon} s^{-1})) and warm white LEDs ($7.76(\pm0.73)\times10^{-7}$ mol_{photon} s^{-1}) is less than 20 % of the photon flux of UV-LEDs ($5.81\pm0.03)\times10^{-6}$ mol_{photon} s^{-1}).

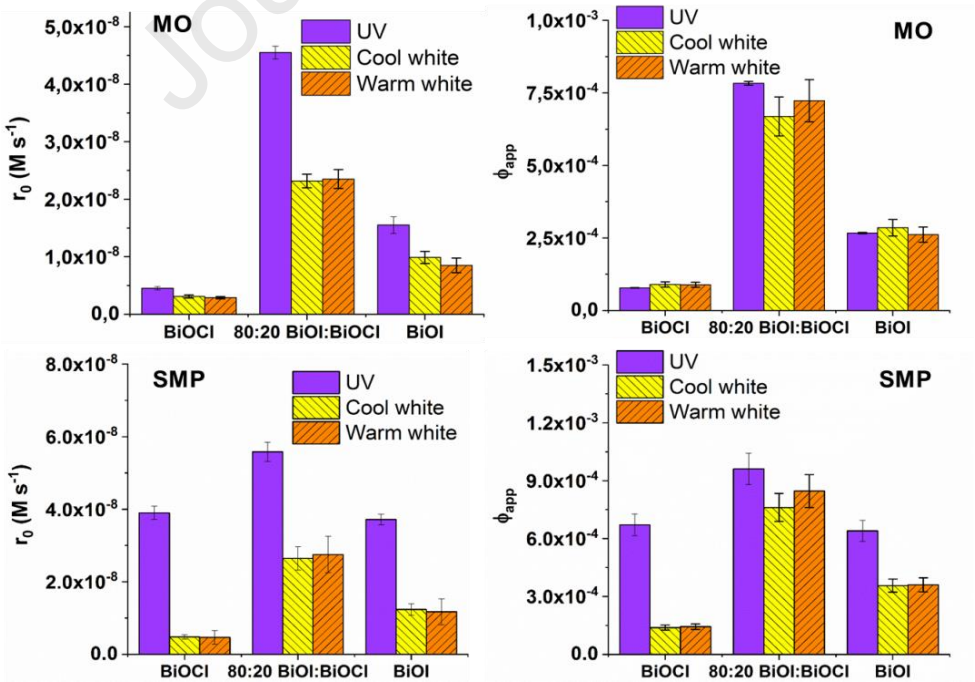

Fig. 3 The initial transformation rate (r_0) and apparent quantum yield (Φ_{app}) of the MO and SMP transformation

In the case of MO using 398 nm light, the value of Φ_{app} was much higher for BiOI than for BiOCl, while for SMP there was no significant difference between them. In the case of MO transformation, the Φ_{app} measured for the composite was nearly double than the Φ_{app} of BiOI, regardless of the light source (Fig 3), and the Φ_{app} for cool and warm white light was just slightly lower than, for 398 nm UV irradiation. This suggests that BiOI and BiOI:BiOCl composite can utilize visible and near-UV light with similar efficiency for the well-absorbed MO transformation. For SMP, both pristine catalysts showed better activity than for MO. The Φ_{app} for 398 nm was higher than for visible light excitation for pristine catalysts, even for BiOCl. Similarly to MO, a significantly increased Φ_{app} values were determined in the case of the composite catalyst and the difference between the values obtained for visible and UV light excitation practically disappeared.

The transformation rate and the Φ_{app} value increases with the catalyst concentration (Fig S3) because the higher surface area increases the number of photogenerated charges. The excellent adsorption properties of the photocatalyst can also contribute to this. Thus, using 1.5 g dm^{-3} BiOI:BiOCl composite suspension, the Φ_{app} determined in 398 nm irradiated suspensions are about three times higher than in the case of 0.5 g dm^{-3} suspensions.

3.7 The role of reactive species

For BiOX photocatalysts, the mechanism of transformation is not yet clear; the OH•-based reaction (Garg et al., 2018a), direct charge transfer (Dai et al., 2007; Garg et al., 2018a) and/or reaction with $O_2^{\bullet-}$ (Yang et al., 2020), as well as photosensitization (Li et al., 2011) were also reported.

Fónagy et al. (2021) evidently demonstrated that 1,4-BQ can be used as e_{cb} scavenger in O_2-free suspension, and the amount of the formed 1,4-H_2Q is proportional to the amount of the photogenerated e_{cb}^-. Thus, we studied the reduction of 1,4-BQ into 1,4-H_2Q in O_2-free and the backward reaction in O_2-saturated suspensions under 398 nm radiation (Fig 4). The transformation of 1,4-H_2Q to 1,4-BQ relates to the reaction with h_{vb}^+, while the reaction between 1,4-H_2Q and $O_2^{\bullet-}$ is responsible mainly for ring-opening processes and mineralization (Fónagy et al., 2021).

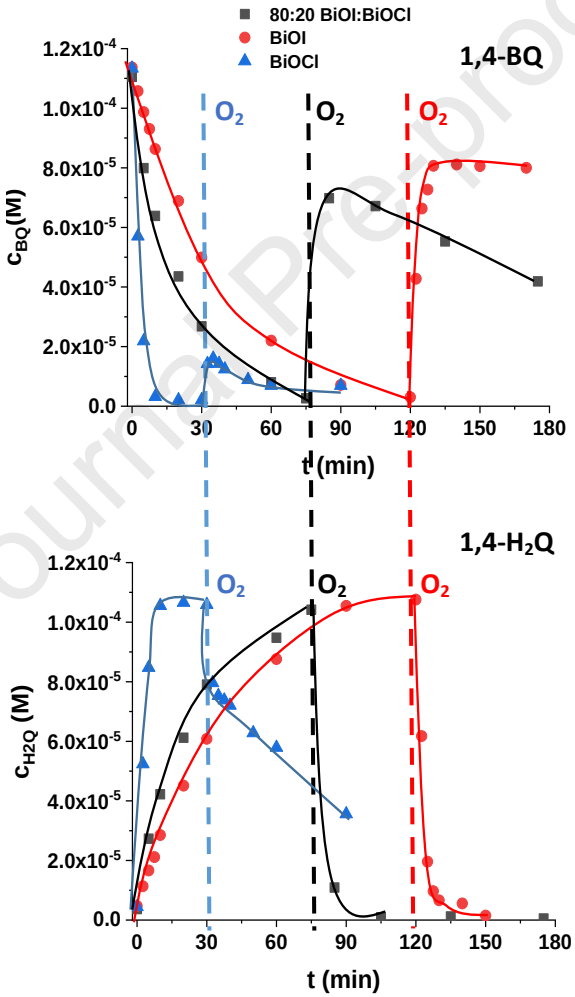

Fig. 4 The concentration of 1,4-BQ and 1,4-H_2Q in O_2-free (before interrupted line) and in O_2 saturated (after interrupted line) suspensions under 398 nm irradiation (interrupted lines show when N_2 bubbling was changed to O_2 bubbling)

The transformation of 1,4-BQ was faster using the composite compared to BiOI, due to the heterojunction between BiOI and BiOCl, which could prevent the charge carrier recombination more efficiently and improve the photocatalytic performance by this way. The 1,4-BQ completely transformed into 1,4-H_2Q in O_2-free suspensions. Replacing N_2 to O_2, 80% (BiOI) and 70% (composite) of H_2Q oxidized back into 1,4-BQ extremely quick, (Fig. 4). The behaviour of BiOCl was quite different: only a small fraction of H_2Q could be transformed back to BQ in O_2-containing suspension, and its transformation takes place, which is most probably caused by the reaction with $O_2^{\bullet-}$ and results in ring-opening products. The transformation of H_2Q in O_2 saturated suspension is negligible for BiOI, but happens for composite (Fig. 4). The UV light induced formation of oxygen vacancies in BiOCl can be the reason of the high activity of BiOCl under 398 nm irradiation, opposite that, the excitation of pure BiOCl (band gap: 3.41 eV, Table 1.) requires radiation with wavelength shorter than 363 nm. The white color of BiOCl to grey changes under 398 nm radiation, which was not observed under visible light radiation.

In agreement with the published results of Fónagy et al. (2020) and Xie et al. (2018) we can conclude that, in O_2 containing suspension of BiOCl, the excitation with 398 nm results in $O_2^{\bullet-}$ formation, which can contribute to the transformation of organic substances. For pure BiOI, there is no $O_2^{\bullet-}$ formation, and the direct charge transfer is responsible for the transformation of organic substances. The improved photocatalytic performance of the composite is due to the combination of the heterojunction between BiOI and BiOCl, and the possibility of $O_2^{\bullet-}$ formation.

In O_2-containing suspensions, methanol (1.0×10^{-2} M) as OH• scavenger does not affect the transformation rate of MO and SMP, even in the case of BiOCl proving that this reactive species has no role in the transformation. Addition of 1,4-BQ (1.0×10^{-2} M) reduced the transformation rate of MO by 84 %, but no effect was observed in the case of SMP. In MO

426 containing suspension the 1,4-BQ transformation was much slower than in SMP containing
427 suspension. The lack of dissolved O_2 also decreased the conversion, but to a different extent:
428 by 70% for well-adsorbed MO and by 34% for poorly adsorbed SMP (Fig. 5). The relatively
429 rapid conversion of SMP in an O_2-free suspension suggests reaction with both photogenerated
430 charges, so SMP partially could take over the role of O_2 as an e_{cb}^- scavenger, which facilitates
431 the reaction with the h_{vb}^+. This is supported by the high value of the rate constant between the
432 sulfonamides and the e_{aq}^- (Mezyk et al., 2007), but further studies are needed to clarify this
433 hypothesis.

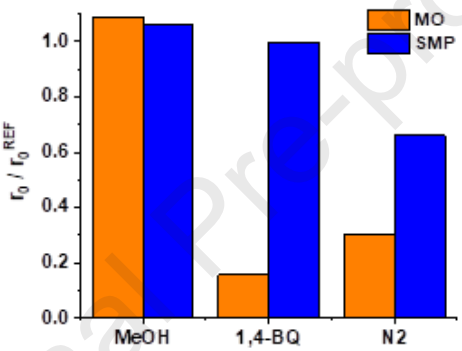

434

435 **Fig. 5** Effect of methanol, 1,4-BQ in air saturated 80:20 BiOI:BiOCl suspensions and the
436 relative transformation rates in O_2-free suspensions

437

438 In the case of BiOI and BiOI:BiOCl photocatalyst, the main product of MO is formed
439 by demethylation (Fig. S6), which confirms the important role of the direct charge transfer in
440 MO conversion (Dai et al., 2007). For TiO_2 P25, the hydroxylation and demethylation occurs
441 parallel (Dai et al., 2007), and both products are formed at a similar rate (Fig. S6). The
442 hydroxylated product results in a red-shift of the UV-Vis spectra, compared to the blue-shift
443 associated with the product formed via demethylation. For SMP the main product is formed
444 via SO_2 extrusion (Khaleel et al., 2013), as LC/MS measurements proved that. The formation
445 of hydroxylated products was not observed for any of the target compounds when BiOI,

BiOCl or composite catalysts were used opposite to the application of P25 (Fig S6). This observation is in agreement with the negligible effect of methanol.

3.8 Reusability of the composite catalyst

The study of the stability and reusability of the catalyst has a crucial role in practical application. Degradation of MO and SMP was monitored for three consecutive cycles (Fig. 6), using the 80:20 BiOI:BiOCl composite catalyst. After complete transformation (end of the cycle), the initial concentration was adjusted to 1.0×10^{-4} M by adding a small volume of concentrated solution. The transformation rate of both target substances decreased after the first cycle, but there was no difference between the values determined for the second and third cycles. Decreased activity may be due to the accumulation of products and their competition with MO and SMP for surface active sites and reactive species. There is no significant change in the XRD patterns after the third cycle; thus, there is probably no change in the photocatalyst structure.

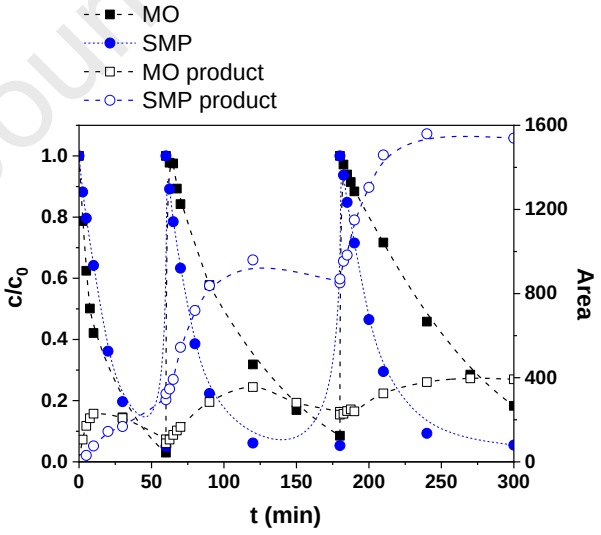

Fig. 6 Transformation of MO and SMP and the formation of their product during three cycles

3.9 Effect of pH, matrix components and matrices

The effect of parameters important for practical applicability, thus pH, Cl (120 mg dm^{-3}), HCO_3 (525 mg dm^{-3}), Na-humate (20 mg dm^{-3}) and two matrices (biologically treated domestic wastewater and river water) on the efficiency was investigated. The concentration of additives was adjusted to the average concentration of biologically treated wastewater. Table S1 shows the chemical parameters of the matrices.

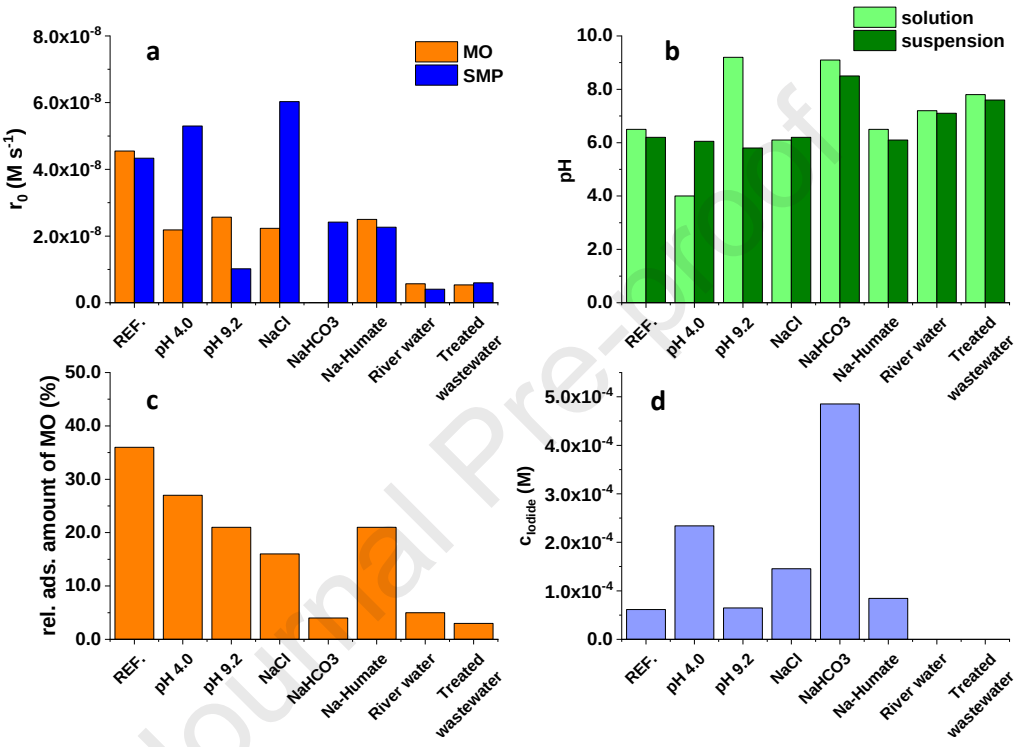

Fig 7 The effect of various matrix components and matrices

a: initial transformation rates; b: pH before and after addition the 80:20 BiOI:BiOCl photocatalyst; c: I concentration after 30 min stirring in dark (determined by spectrophotometry); d: relative amount of adsorbed MO (in the case of real matrices could not be determined due to matrix absorption)

The pH of the solution was adjusted to 9.2 and 4.0 with NaOH and H_2SO_4 solutions, respectively. The addition of BiOI:BiOCl catalyst restored the pH of the suspension to around 6.5. The protonation-deprotonation process of MO (pKa = 3.46) could not affect its adsorption. Nevertheless, the relative amount of adsorbed MO (from 36% to 21% and 27%) and the conversion rate (to 45% and 53%) was significantly reduced (Fig 7). The ionic

components can change the surface properties and electrostatic attraction between photocatalyst and substrate, thereby affect the photodegradation. NaCl decreased the adsorption of MO (to 16%) and its conversion rate (to 49%), but increased the transformation rate of SMP (by 46%). A significant change was observed when 525 mg dm^{-3} $NaHCO_3$ was added to the suspension. The transformation rate of MO was completely and of SMP partly (to 58%) inhibited. MO practically did not adsorb in this case. Spectrophotometric measurements show that the concentration of I^- in the solution did not change due to the addition of NaOH, but H_2SO_4 and NaCl, and even $NaHCO_3$ increased that, suggesting a change in the surface of the catalyst (Fig 7). The relative high I^- concentration in the suspension proved that HCO_3^- dramatically changed the photocatalyst. To accurately explain these results, further studies are needed on the effect of different ions on the surface properties and stability of the BiOI:BiOCl photocatalyst.

The humic acids and humates often compete for adsorption sites with the pollutants. As our results show, humate decreased the transformation of MO and SMP to a similar extent. I^- leaching was not observed, but the relative adsorbed amount of MO decreased to 21 % (Fig 7). Using river water and biologically treated domestic wastewater, the joined effect of various inorganic and organic components practically completely inhibited the elimination of both test substances. Our results suggest that despite their excellent adsorption and photocatalytic properties, our knowledge of the stability of BiOI:BiOCl photocatalyst and the effect of each matrix component and matrices are incomplete and require further investigation.

3.10 Toxicity assay

Toxicity studies were performed to check the environmentally friendly use of the prepared photocatalyst. The toxicity of the composite photocatalyst and the treated MO and

SMP solution was determined using the *Vibrio fischeri* test organism; the inhibition of the emitted luminescent light intensity is proportional to the degree of toxicity.

The toxicity of 80:20 BiOI:BiOCl photocatalyst was determined during 90 min radiation without organic substances. After removing the catalyst particles, there was no significant effect of the filtered solutions on the test organism. The inhibition effect was less than 10 % and proved that no harmful substances are leached from the catalyst particles (Fig. 7).

The toxicity of 1.0×10^{-4} M MO and SMP solutions was negligible. Although the photocatalyst does not pose a risk to the environment, the conversion of both organic substances significantly increased the degree of inhibition effect, most probably due to the formation of highly toxic intermediates. Our results underline that the toxicity of the formed products during the transformation of each model compound should be given priority. However, for other target compounds, the use of the photocatalyst tested here may be appropriate to remove them without increasing toxicity. All this requires further investigations using various target substances.

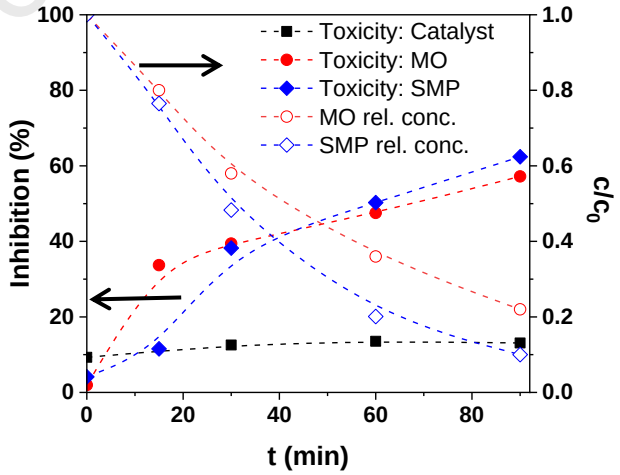

Fig. 8 The change of MO and SMP relative concentration (1.0×10^{-4} M) and the degree of the inhibition, using 80:20 BiOI:BiOCl photocatalyst (0.5 g dm^{-3}) suspension

3.6 Comparison of the efficiency of BiOI:BiOCl and Aeroxide P25 TiO_2

Aeroxide P25 TiO_2 is often used as a "reference" in the case of heterogeneous photocatalysis. The prepared composite photocatalyst efficiency was compared to this widely used, commercially available, well-known material. The photocatalysts (1.5 g dm^{-3}) and MO (1.0×10^{-4} M) concentrations were the same in both cases. The relative amount of adsorbed MO was not significant for TiO_2 (6 %) comparing to that measured for 80:20 BiOI:BiOCl photocatalyst (75 %).

Different light sources were applied for the excitation; mercury vapor lamp emitting in the range of 300 - 400 nm, $5.13(\pm0.34)\times10^{7}$ mol_{photon} s^{1} for the TiO_2 and 398 nm UV LED, $5.81(\pm0.03)\times10^{-6}$ mol_{photon} s^{-1} for the composite photocatalyst). The electric energy required to degrade the concentration by one order of magnitude in a unit volume (100 cm^3) was calculated and used for comparison. This value depends not only on the catalyst activity but also on the parameters of the light source. For the calculation, the volume of the treated suspension, the electrical parameters of the light sources, and the time required for the 90% decomposition were used. Using 0.5 g dm^{-3} 80:20 BiOI:BiOCl photocatalyst, this value was 30, and 40 kJ for UV LED and for visible light LEDs, respectively. Similar values (24 and 32 kJ) was determined for SMP. At 1.5 g dm^{-3} concentration of photocatalyst, 30 and 24 kJ decreased to ~12 kJ, about half of the energy requirement calculated for TiO_2 (23 kJ), using 15 W mercury-vapor lamp and the same concentration of photocatalyst.

CONCLUSIONS

This study aims to investigate the absorption capacity and activity of BiOCl, BiOI, and BiOI:BiOCl composites for elimination two organic substances MO and SPM. Three light sources were used and compared to decompose MO and SMP as a model compounds: 398 nm UV, cool and warm white visible light LEDs. BiOI and BiOI:BiOCl composites were

effective photocatalysts under near-UV and visible light; the best results were obtained using the 80:20 BiOI: BiOCl composite, which showed a similar adsorption capacity as BiOI, but the initial transformation rate of MO was about three times higher than for pure BiOI. There was a significant difference between the light sources' photon flux and the average energy of the emitted photons of the applied LEDs. Thus the comparison was based on the Φ_{app} values of transformation. In the case of the BiOI and BiOI:BiOCl composite, the obtained Φ_{app} values were similar for the UV, cool white, and warm white LEDs. All this suggests that BiOI:BiOCl composite can utilize visible and ultraviolet light with similar efficiency.

The reusability was studied during three consecutive cycles, in Milli-Q water. The transformation rate decreased after the first one, but there was no difference between the transformation rates determined in the second and third cycles. The decreased efficiency probably relates to the accumulation of intermediates on the surface. However, the catalyst does not pose a risk to the environment; the conversion of MO and SMP results in toxic intermediates. Prolonged treatment time is likely to result in the degradation of intermediates and reduction of toxicity.

According to the transformation of 1,4-BQ, the effect of radical scavengers, and formed intermediates, the main transformation way could be the direct charge transfer in both cases, which results in demethylation of MO and SO_2 extrusion from SMP. An interesting spectral feature was observed for pure BiOCl; its light absorption extends in the visible region due to the UV light induced formation of oxygen vacancies. This can be the reason of that, under 398 nm irradiation BiOCl showed high activity for the transformation of 1,4-BQ and for SMP opposite that its band gap value is 3.41 eV. It was not observed under visible light radiation.

Using 1.5 g dm^{-3} concentration of the 80:20 BiOI:BiOCl photocatalyst and UV LED emitting at 398 nm, the energy requirement of conversion was significantly lower than for the

575 widely used TiO_2 photocatalyst under 300 - 400 nm UV irradiation, using a mercury-vapor
576 lamp. All this proves that combining these composite catalysts with LED technology can be
577 an energy-efficient solution for removing the well-adsorbed dyes from water. However, the
578 negative effect of the matrix component, especially HCO_3^-, raises some questions for
579 practical applicability. Based on these, in the case of wastewaters, pre-treatment can be an
580 essential factor for the efficient application of the investigated photocatalysts.
581
582 **FUNDING**
583 This work was supported by the János Bolyai Research Scholarship of the Hungarian
584 Academy of Sciences, and the new national excellence program of the Ministry for
585 Innovation and Technology (ÚNKP-20-3-SZTE 548, and ÚNKP-20-5-SZTE 639). The
586 research work was sponsored by the National Research, Development and Innovation Office
587 (NKFIH), project number FK 132742.
588
589 **DECLARATIONS OF INTEREST**
590 The authors declare that they have no known competing financial interests or personal
591 relationships that could have influenced the work reported in this paper.
592
593 **REFERENCES**
594 Ahern, J.C., Fairchild, R., Thomas, J.S., Carr, J., Patterson, H.H., 2015. Characterization of
595 BiOX compounds as photocatalysts for the degradation of pharmaceuticals in water.
596 Appl. Catal. B Environ. 179, 229–238. https://doi.org/10.1016/j.apcatb.2015.04.025
597 Ahmed, S.N., Haider, W., 2018. Heterogeneous photocatalysis and its potential applications
598 in water and wastewater treatment: A review. Nanotechnology 29.
599 https://doi.org/10.1088/1361-6528/aac6ea
600 Akpan, U.G., Hameed, B.H., 2009. Parameters affecting the photocatalytic degradation of

dyes using TiO2-based photocatalysts: A review. J. Hazard. Mater. https://doi.org/10.1016/j.jhazmat.2009.05.039

Bárdos, E., Király, A.K., Pap, Z., Baia, L., Garg, S., Hernádi, K., 2019. The effect of the synthesis temperature and duration on the morphology and photocatalytic activity of BiOX (X = Cl, Br, I) materials. Appl. Surf. Sci. 479, 745–756. https://doi.org/10.1016/j.apsusc.2019.02.136

Chen, J., Loeb, S., Kim, J.H., 2017. LED revolution: Fundamentals and prospects for UV disinfection applications. Environ. Sci. Water Res. Technol. 3, 188–202. https://doi.org/10.1039/c6ew00241b

Cheng, H., Huang, B., Dai, Y., 2014. Engineering BiOX (X = Cl, Br, I) nanostructures for highly efficient photocatalytic applications. Nanoscale 6, 2009–2026. https://doi.org/10.1039/c3nr05529a

Cornet, J.F., Marty, A., Gros, J.B., 1997. Revised technique for the determination of mean incident light fluxes on photobioreactors. Biotechnol. Prog. 13, 408–415. https://doi.org/10.1021/bp970045c

Dai, G., Yu, J., Liu, G., 2011. Synthesis and enhanced visible-light photoelectrocatalytic activity of p - N junction BiOI/TiO2 nanotube arrays. J. Phys. Chem. C 115, 7339–7346. https://doi.org/10.1021/jp200788n

Dai, K., Chen, H., Peng, T., Ke, D., Yi, H., 2007. Photocatalytic degradation of methyl orange in aqueous suspension of mesoporous titania nanoparticles. Chemosphere 69, 1361–1367. https://doi.org/10.1016/j.chemosphere.2007.05.021

Di, J., Xia, J., Ji, M., Xu, L., Yin, S., Zhang, Q., Chen, Z., Li, H., 2016. Carbon quantum dots in situ coupling to bismuth oxyiodide via reactable ionic liquid with enhanced photocatalytic molecular oxygen activation performance. Carbon N. Y. 98, 613–623. https://doi.org/10.1016/j.carbon.2015.11.015

626 Dong, F., Sun, Y., Fu, M., Wu, Z., Lee, S.C., 2012. Room temperature synthesis and highly
627 enhanced visible light photocatalytic activity of porous BiOI/BiOCl composites
628 nanoplates microflowers. J. Hazard. Mater. 219–220, 26–34.
629 https://doi.org/10.1016/j.jhazmat.2012.03.015
630 Flak, D., Braun, A., Mun, B.S., Park, J.B., Parlinska-Wojtan, M., Graule, T., Rekas, M., 2013.
631 Spectroscopic assessment of the role of hydrogen in surface defects, in the electronic
632 structure and transport properties of TiO2, ZnO and SnO2 nanoparticles. Phys. Chem.
633 Chem. Phys. 15, 1417–1430. https://doi.org/10.1039/c2cp42601c
634 Fónagy, O., Szabó-Bárdos, E., Horváth, O., 2021. 1,4-Benzoquinone and 1,4-hydroquinone
635 based determination of electron and superoxide radical formed in heterogeneous
636 photocatalytic systems. J. Photochem. Photobiol. A Chem. 407.
637 https://doi.org/10.1016/j.jphotochem.2020.113057
638 Ganose, A.M., Cuff, M., Butler, K.T., Walsh, A., Scanlon, D.O., 2016. Interplay of Orbital
639 and Relativistic Effects in Bismuth Oxyhalides: BiOF, BiOCl, BiOBr, and BiOI. Chem.
640 Mater. 28, 1980–1984. https://doi.org/10.1021/acs.chemmater.6b00349
641 Garg, S., Yadav, M., Chandra, A., Sapra, S., Gahlawat, S., Ingole, P.P., Pap, Z., Hernadi, K.,
642 2018a. Biofabricated BiOI with enhanced photocatalytic activity under visible light
643 irradiation. RSC Adv. 8, 29022–29030. https://doi.org/10.1039/c8ra05661g
644 Garg, S., Yadav, M., Chandra, A., Sapra, S., Gahlawat, S., Ingole, P.P., Todea, M., Bardos,
645 E., Pap, Z., Hernadi, K., 2018b. Facile green synthesis of BiOBr nanostructures with
646 superior visible-light-driven photocatalytic activity. Materials (Basel). 11.
647 https://doi.org/10.3390/ma11081273
648 Hao, L., Huang, H., Guo, Y., Du, X., Zhang, Y., 2017. Bismuth oxychloride homogeneous
649 phasejunction BiOCl/Bi 12 O 17 Cl 2 with unselectively efficient photocatalytic activity
650 and mechanism insight. Appl. Surf. Sci. 420, 303–312.

https://doi.org/10.1016/j.apsusc.2017.05.076

Hatchard, C.G., Parker, C.A., 1956. A new sensitive chemical actinometer - II. Potassium ferrioxalate as a standard chemical actinometer. Proc. R. Soc. London. Ser. A. Math. Phys. Sci. 235, 518–536. https://doi.org/10.1098/rspa.1956.0102

Jia, X., Cao, J., Lin, H., Chen, Y., Fu, W., Chen, S., 2015. One-pot synthesis of novel flower-like BiOBr0.9I0.1/BiOI heterojunction with largely enhanced electron-hole separation efficiency and photocatalytic performances. J. Mol. Catal. A Chem. 409, 94–101. https://doi.org/10.1016/j.molcata.2015.08.008

Jiang, Y.R., Lin, H.P., Chung, W.H., Dai, Y.M., Lin, W.Y., Chen, C.C., 2015. Controlled hydrothermal synthesis of BiOxCly/BiOmIn composites exhibiting visible-light photocatalytic degradation of crystal violet. J. Hazard. Mater. 283, 787–805. https://doi.org/10.1016/j.jhazmat.2014.10.025

Jo, W.K., Tayade, R.J., 2014. New generation energy-efficient light source for photocatalysis: LEDs for environmental applications. Ind. Eng. Chem. Res. 53, 2073–2084. https://doi.org/10.1021/ie404176g

Khaleel, N.D.H., Mahmoud, W.M.M., Hadad, G.M., Abdel-Salam, R.A., Kümmerer, K., 2013. Photolysis of sulfamethoxypyridazine in various aqueous media: Aerobic biodegradation and identification of photoproducts by LC-UV-MS/MS. J. Hazard. Mater. 244–245, 654–661. https://doi.org/10.1016/j.jhazmat.2012.10.059

Khan, J.A., Sayed, M., Khan, S., Shah, N.S., Dionysiou, D.D., Boczkaj, G., 2019. Advanced oxidation processes for the treatment of contaminants of emerging concern, Contaminants of Emerging Concern in Water and Wastewater: Advanced Treatment Processes. Elsevier Inc. https://doi.org/10.1016/B978-0-12-813561-7.00009-2

Konstantinou, I.K., Albanis, T.A., 2003. Photocatalytic transformation of pesticides in aqueous titanium dioxide suspensions using artificial and solar light: Intermediates and

degradation pathways. Appl. Catal. B Environ. 42, 319–335. https://doi.org/10.1016/S0926-3373(02)00266-7

Kuhn, H.J., Braslavsky, S.E., Schmidt, R., 2004. INTERNATIONAL UNION OF PURE AND APPLIED CHEMISTRY - Chemical Actinometry. IUPAC Tech. Rep. 1–47.

Li, T.B., Chen, G., Zhou, C., Shen, Z.Y., Jin, R.C., Sun, J.X., 2011. New photocatalyst BiOCl/BiOI composites with highly enhanced visible light photocatalytic performances. Dalt. Trans. 40, 6751–6758. https://doi.org/10.1039/c1dt10471c

Liu, C., Wang, X.J., 2016. Room temperature synthesis of Bi4O5I2 and Bi5O7I ultrathin nanosheets with a high visible light photocatalytic performance. Dalt. Trans. 45, 7720–7727. https://doi.org/10.1039/c6dt00530f

Liu, Z., Wang, Q., Tan, X., Wang, Y., Jin, R., Gao, S., 2019. Enhanced photocatalytic performance of TiO2 NTs decorated with chrysanthemum-like BiOI nanoflowers. Sep. Purif. Technol. 215, 565–572. https://doi.org/10.1016/j.seppur.2019.01.046

Mezyk, S.P., Neubauer, T.J., Cooper, W.J., Peller, J.R., 2007. Free-radical-induced oxidative and reductive degradation of sulfa drugs in water: Absolute kinetics and efficiencies of hydroxyl radical and hydrated electron reactions. J. Phys. Chem. A 111, 9019–9024. https://doi.org/10.1021/jp073990k

Qian, R., Zong, H., Schneider, J., Zhou, G., Zhao, T., Li, Y., Yang, J., Bahnemann, D.W., Pan, J.H., 2019. Charge carrier trapping, recombination and transfer during TiO2 photocatalysis: An overview. Catal. Today 335, 78–90. https://doi.org/10.1016/j.cattod.2018.10.053

Sergejevs, A., Clarke, C.T., Allsopp, D.W.E., Marugan, J., Jaroenworaluck, A., Singhapong, W., Manpetch, P., Timmers, R., Casado, C., Bowen, C.R., 2017. A calibrated UV-LED based light source for water purification and characterisation of photocatalysis. Photochem. Photobiol. Sci. 16, 1690–1699. https://doi.org/10.1039/c7pp00269f

Shan, L., Bi, J., Liu, Y., 2018. Roles of BiOCl(001) in face-to-faced BiOI(010)/BiOCl(001) heterojunction. J. Nanoparticle Res. 20. https://doi.org/10.1007/s11051-018-4272-9

Shen, F., Zhou, L., Shi, J., Xing, M., Zhang, J., 2015. Preparation and characterization of SiO2/BiOX (X = Cl, Br, I) films with high visible-light activity. RSC Adv. 5, 4918–4925. https://doi.org/10.1039/c4ra10227d

Siao, C.W., Chen, H.L., Chen, L.W., Chang, J.L., Yeh, T.W., Chen, C.C., 2018. Controlled hydrothermal synthesis of bismuth oxychloride/bismuth oxybromide/bismuth oxyiodide composites exhibiting visible-light photocatalytic degradation of 2-hydroxybenzoic acid and crystal violet. J. Colloid Interface Sci. 526, 322–336. https://doi.org/10.1016/j.jcis.2018.04.097

Singh, S., Sharma, R., Khanuja, M., 2018. A review and recent developments on strategies to improve the photocatalytic elimination of organic dye pollutants by BiOX (X=Cl, Br, I, F) nanostructures, Korean Journal of Chemical Engineering. https://doi.org/10.1007/s11814-018-0112-y

Stefan, M.I., 2017. Advanced Oxidation Processes for Water Treatment - Fundamentals and Applications , Water Intelligence Online. https://doi.org/10.2166/9781780407197

Tauc, J., 1968. Optical properties and electronic structure of amorphous Ge and Si. Mater. Res. Bull. 3, 37–46. https://doi.org/10.1016/0025-5408(68)90023-8

Wang, J., Huang, Y., Guo, J., Zhang, J., Wei, X., Ma, F., 2020. Optoelectronic response and interfacial properties of BiOI/BiOX (X=F, Cl, Br) heterostructures based on DFT investigation. J. Solid State Chem. 284. https://doi.org/10.1016/j.jssc.2020.121181

Wegner, E.E., Adamson, A.W., 1966. Photochemistry of Complex Ions. III. Absolute Quantum Yields for the Photolysis of Some Aqueous Chromium(III) Complexes. Chemical Actinometry in the Long Wavelength Visible Region. J. Am. Chem. Soc. 88, 394–404. https://doi.org/10.1021/ja00955a003

Wu, L., Zhang, Q., Li, Z., Liu, X., 2020. Mechanochemical syntheses of a series of bismuth oxyhalide composites to progressively enhance the visible-light responsive activities for the degradation of bisphenol-A. Mater. Sci. Semicond. Process. 105. https://doi.org/10.1016/j.mssp.2019.104733

Xiao, X., Hao, R., Liang, M., Zuo, X., Nan, J., Li, L., Zhang, W., 2012. One-pot solvothermal synthesis of three-dimensional (3D) BiOI/BiOCl composites with enhanced visible-light photocatalytic activities for the degradation of bisphenol-A. J. Hazard. Mater. 233–234, 122–130. https://doi.org/10.1016/j.jhazmat.2012.06.062

Xiao, X., Liu, C., Zuo, X., Liu, J., Nan, J., 2016. Microwave synthesis of hierarchical BiOCl microspheres as a green adsorbent for the pH-dependent adsorption of methylene blue. J. Nanosci. Nanotechnol. 16, 12517–12525. https://doi.org/10.1166/jnn.2016.12969

Yang, C., Li, F., Zhang, M., Li, T., Cao, W., 2016. Preparation and first-principles study for electronic structures of BiOI/BiOCl composites with highly improved photocatalytic and adsorption performances. J. Mol. Catal. A Chem. 423, 1–11. https://doi.org/10.1016/j.molcata.2016.06.007

Yang, J., Xie, T., Zhu, Q., Wang, J., Xu, L., Liu, C., 2020. Boosting the photocatalytic activity of BiOX under solar light: Via selective crystal facet growth. J. Mater. Chem. C 8, 2579–2588. https://doi.org/10.1039/c9tc05752h

Yao, S., Wang, J., Zhou, X., Zhou, S., Pu, X., Li, W., 2020. One-pot low-temperature synthesis of BiOX/TiO2 hierarchical composites of adsorption coupled with photocatalysis for quick degradation of colored and colorless organic pollutants. Adv. Powder Technol. 31, 1924–1932. https://doi.org/10.1016/j.apt.2020.02.023

Yusoff, M.A.M., Imam, S.S., Shah, I., Adnan, R., 2019. Photocatalytic activity of bismuth oxyiodide nanospheres and nanoplates in the degradation of ciprofloxacin under visible light. Mater. Res. Express 6. https://doi.org/10.1088/2053-1591/ab2918

751 Zhang, F., Chen, X., Wu, F., Ji, Y., 2016. High adsorption capability and selectivity of ZnO
752 nanoparticles for dye removal. Colloids Surfaces A Physicochem. Eng. Asp. 509, 474–
753 483. https://doi.org/10.1016/j.colsurfa.2016.09.059
754 Zhang, Y., Zhang, J., Tang, W., Wang, N., Liu, Y., Guo, H., 2020. Preparation and
755 characterization of hierarchical BiO0.5Cl0.5 with excellent adsorption and photocatalytic
756 abilities for removal of aquatic dyes. Desalin. WATER Treat. 201, 356–368.
757 https://doi.org/10.5004/dwt.2020.25866
758 Zhao, Q., Xing, Y., Liu, Z., Ouyang, J., Du, C., 2018. Synthesis and Characterization of
759 Modified BiOCl and Their Application in Adsorption of Low-Concentration Dyes from
760 Aqueous Solution. Nanoscale Res. Lett. 13. https://doi.org/10.1186/s11671-018-2480-y
761 Zhong, Y., Liu, Y., Wu, S., Zhu, Y., Chen, H., Yu, X., Zhang, Y., 2018. Facile fabrication of
762 BiOI/BiOCl immobilized films with improved visible light photocatalytic performance.
763 Front. Chem. 6, 1–11. https://doi.org/10.3389/fchem.2018.00058
764

765 **SUPPLEMENTARY**

766 **Table S1.** The chemical parameters of the water-matrices

Parameter	River water (River Tisza, Hungary)	Biologically treated domestic wastewater
pH	7.2	7.8
Conductivitiy (µS cm^{-1})	671	1258
COD (mg dm^{-3})	12.8	24.4
NH_4^+–N (mg dm^{-3})	< 0.4	< 0.4
NO_3^- (mg dm^{-3})	7.84	3.37
Cl^- (mg dm^{-3})	no data	120
TOC (mg dm^{-3})	3.8	6.9
HCO_3^- (mg dm^{-3})	148	525

767

768

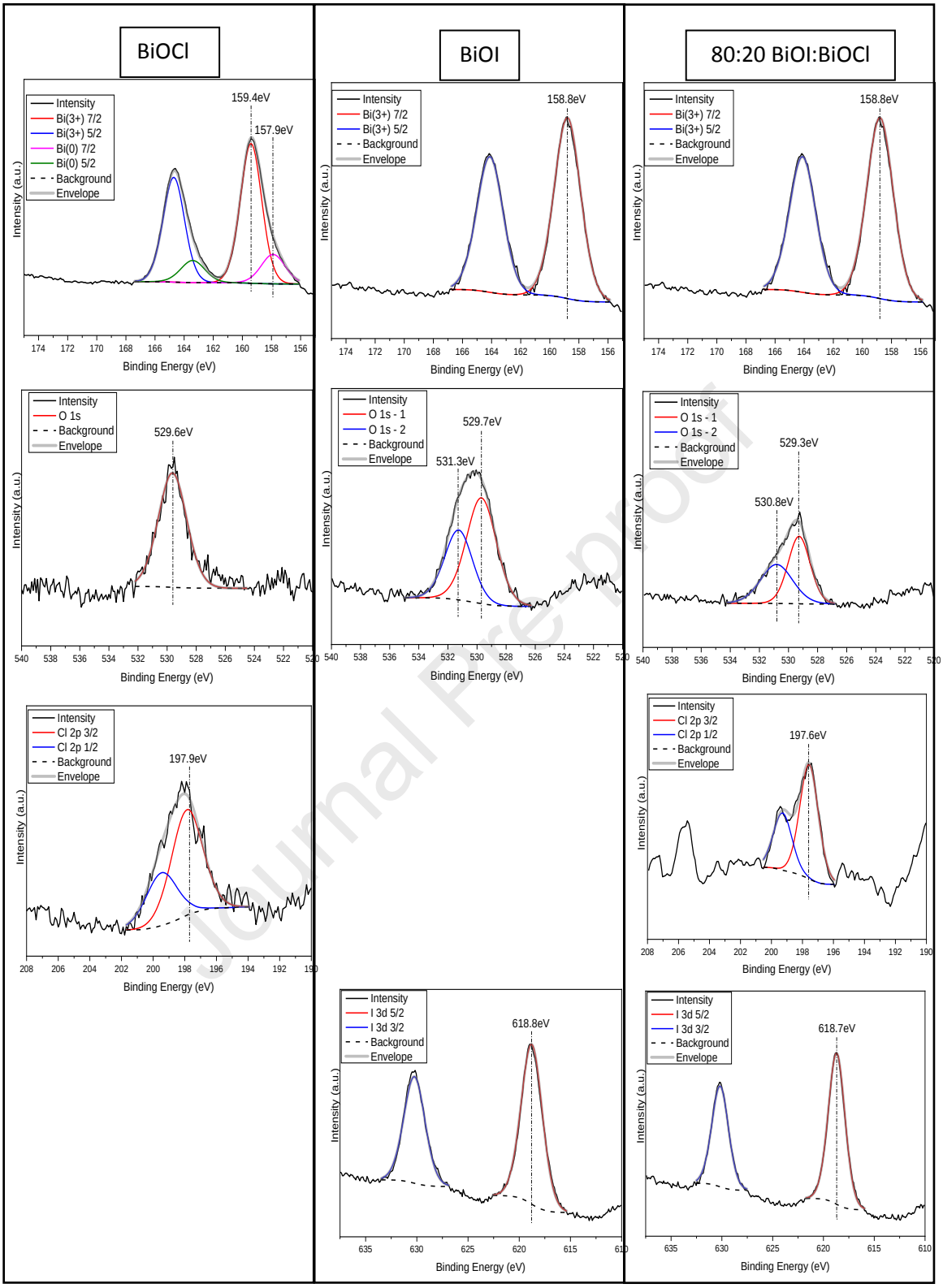

Fig. S1 High resolution X-ray photoelectron spectroscopy (XPS) spectra of elements (Bi 4f; O 1s; I 3d and Cl 2p) of BiOI, BiOCl and 80:20 BiOI:BiOCl composite

Evaluation of XPS results:

The peaks with the binding energies of 158.8 and 167.7 eV are attributed to Bi $4f_{7/2}$ and Bi $4f_{5/2}$, respectively, and represent the typical Bi^{3+}. A reduced/metallic component is caused by the X-ray source during the measurement and can be observed only in the case of BiOCl. Lower binding energy oxygen peak component (O1s) refers to the lattice oxygen in the $(BiO)_2^{2+}$, higher binding energy peak is attributed to the surface hydroxyl groups (Liu and Wang, 2016). For BiOCl only the lattice oxygen was observed, while for BiOI and composite both peaks appear. The peak of Cl $2p_{3/2}$ at 197.9 eV (197.6 eV in the composite) corresponds to Cl^- (Hao et al., 2017). The anomalous background of the Cl 2p spectra is due to the neighboring Bi 4f peaks. The peaks of I 3d can be found at 630.0 and 618.8 eV, and attributed to I $3d_{3/2}$ and I $3d_{5/2}$, respectively, corresponding to I^- in the BiOI (Di et al., 2016).

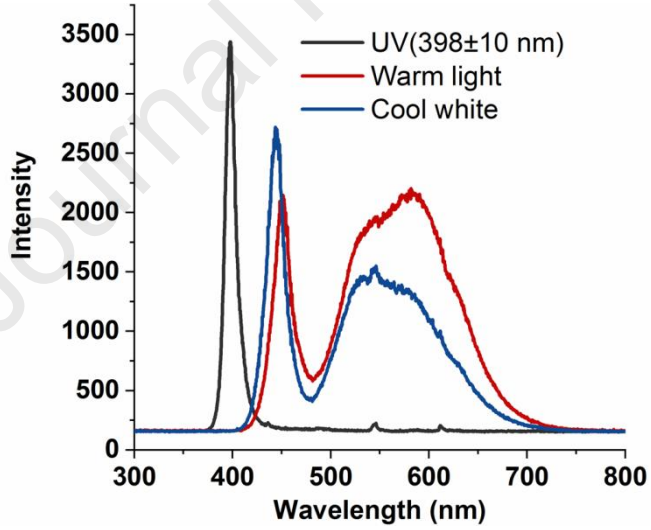

Fig S2 The The spectra of the LED light sources

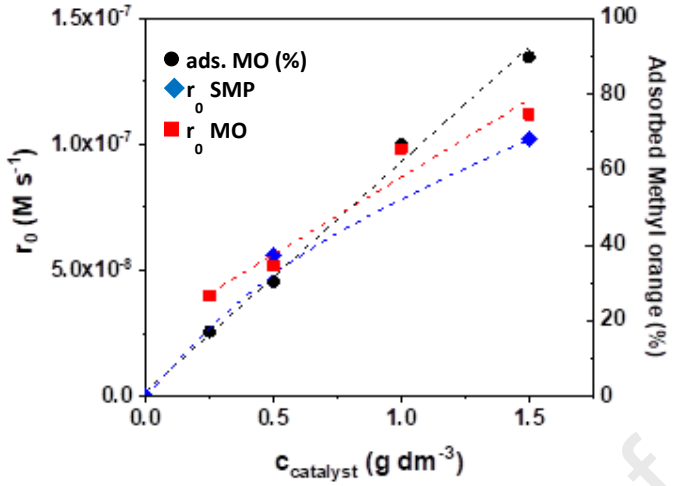

811

812 **Fig. S3** The effect of the 80:20 BiOI:BiOCl catalyst dosage on the relative adsorbed amount

813 (%) and initial transformation rate of methyl orange (2.0×10^{-4} M)

814

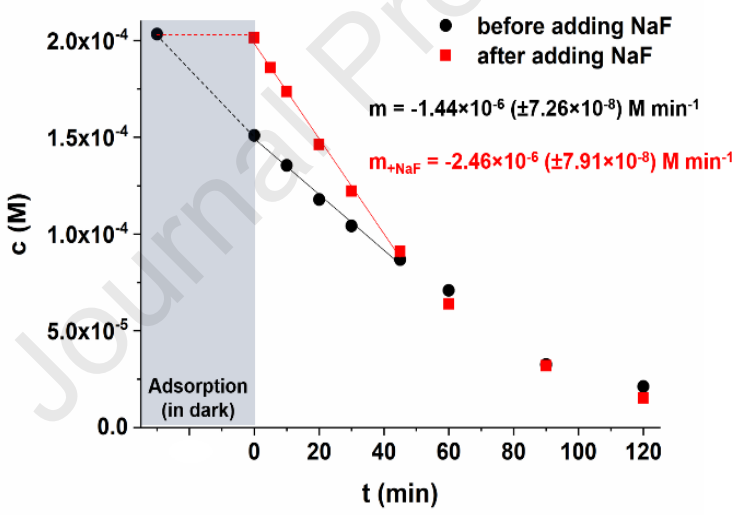

815

816 **Fig. S4** The concentration of methyl orange as a function of time with and without the

817 addition of fluoride ions (80:20 BiOI:BiOCl, UV-LED)

818

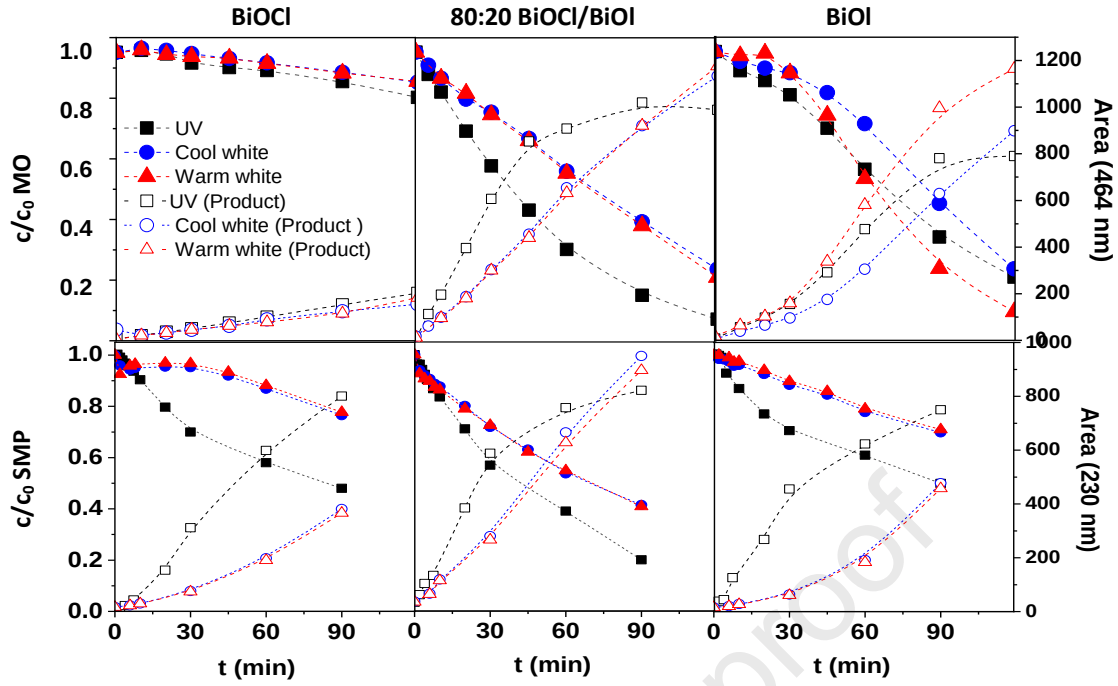

Fig. S5 The relative concentration of MO and SMP, and their primary products versus time of treatment (a: MO+BiOCl; b: MO+80:20 BiOI:BiOCl composite; c: MO+BiOI, d: SMP+BiOCl; e: SMP+80:20 BiOI:BiOCl composite; f: SMP+BiOI) using various light sources

825

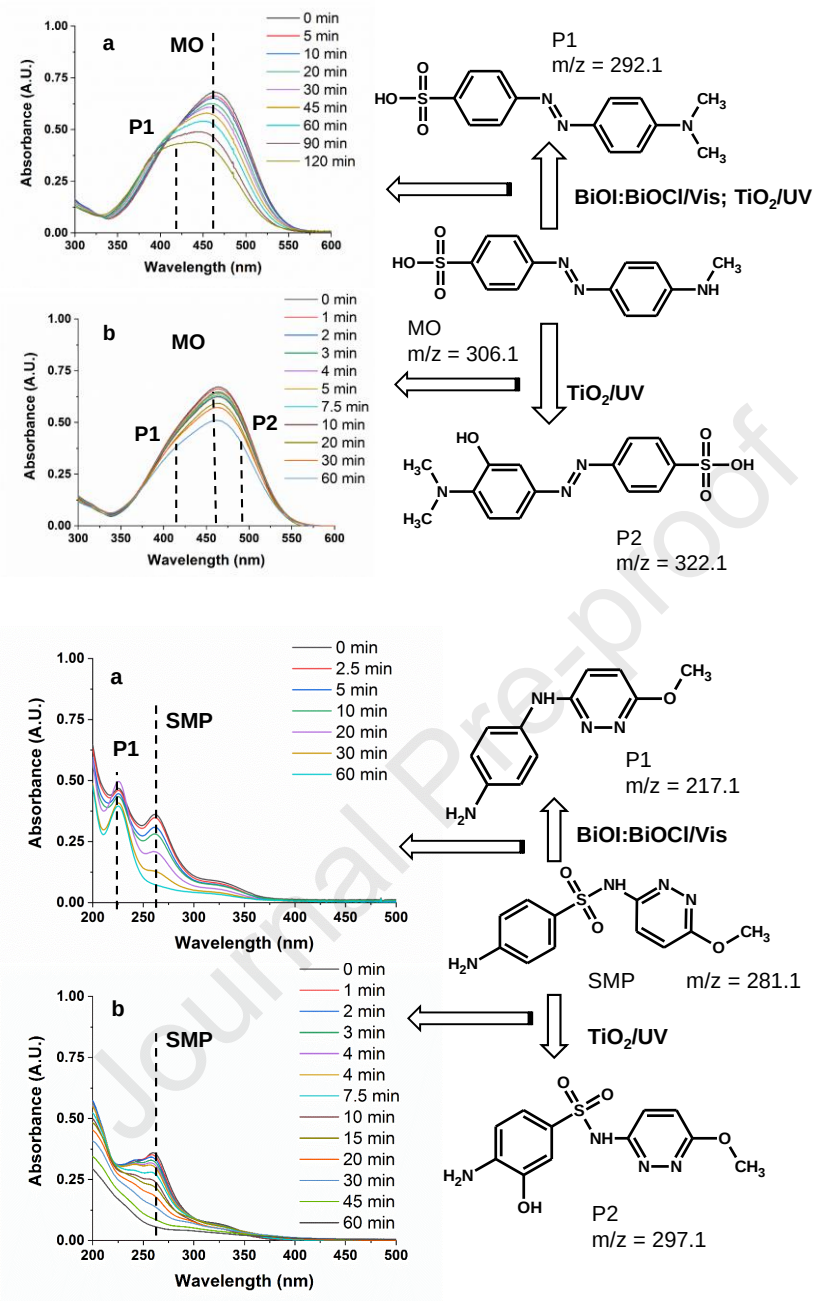

826

827 **Fig. S6** The spectra of the treated solutions using 80:20 BiOI/BIOCl composite (a) and P25
828 photocatalysts (b), and the chemical structure of the products determined by HPLC-MS

829

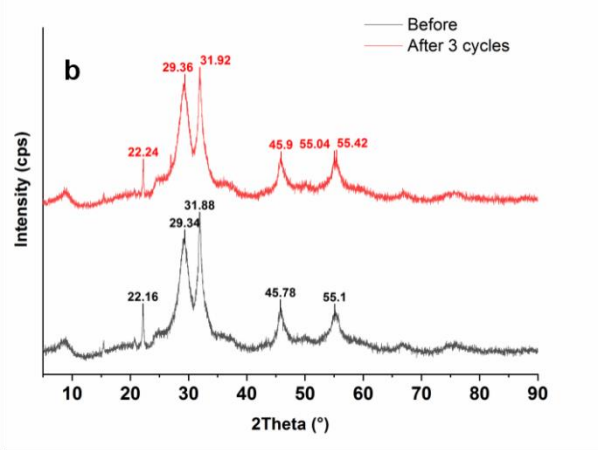

Fig. S7 The XRD patterns of the 80:20 BiI:BiOCl catalyst before and after the three cycle

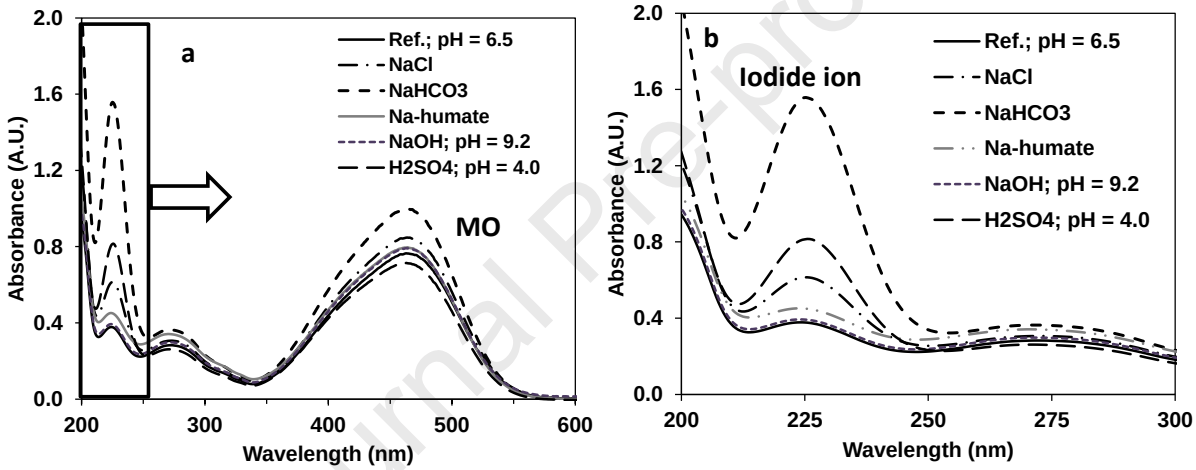

Fig S8 Effect of pH and matrix components on the iodide ion leaching from the 80:20 BIOI:BiOCl photocatalyst. The UV spectrum of the suspensions after stirring for 30 minutes in dark

Declaration of interests

☒ The authors declare that they have no known competing financial interests or personal relationships that could have appeared to influence the work reported in this paper.

☐The authors declare the following financial interests/personal relationships which may be considered as potential competing interests: